MARS 2001 ODYSSEY

GAMMA RAY SPECTROMETER

HIGH ENERGY NEUTRON DETECTOR DATA PROCESSING

Version 1.2

06/06/2006

Prepared By:
M.L. Litvik and I. Mitrofanov
Institute for Space Research
Russian Academy of Science

Table of Contents

1. Introduction 3
2. Level 0 Processing- Spacecraft Data Receipt and Storage 5
2.1. GRS_tl 5
2.2. GRS Displays 6
3. Level 1-A Processing – Timing and Spatial Information 6
3.1. SPICE Processes 6
4. Level 1-B Processing – Background Subtracted Data 7
4.1. Background Subtraction 7
4.2. Extraction of Solar Particle Events 8
5. Level 1-C Processing – Spatially and Temporally Binned Data 9
5.1. Averaged Normalized Relative Counting Rates 9
5.2. Normalization to Solis Planum 11
5.3. Normalized Map Verification 12
5.4. Neutron Flux Maps 13
5.4.1. HEND Detector Efficiency Functions 13
5.4.2. Deconvolution of Neutron Spectra 14
5.4.3. Verification of Neutron Fluxes 16
6. Appendix 1 - Calculation of Normalized Counting Rate Uncertainties 19
7. Appendix 2 - Corrections to HEND AHD & DHD data products 22

1. INTRODUCTION

The Mars Odyssey Gamma-Ray Spectrometer (GRS) is a suite of three instruments working together to collect geochemical data from the surface of Mars. The instruments are the University of Arizona (UA) gamma subsystem (GS), the Los Alamos National Laboratory (LANL) neutron spectrometer (NS), and the Russian Institute of Space Sciences (IKI) high-energy neutron detector (HEND). The instruments are complimentary in that the neutron instruments have much better counting statistics and can sample to greater depths than the GS, but the GS determines the abundances of many more elements. A full accounting of the GRS instrument suite can be found in Boynton et al., 2004. The purpose of this document is to describe each step in the HEND data reduction algorithms from data receipt through calculation of temporally and spatially binned neutron fluxes.

The HEND instrument is composed of five detectors that provide measurements of neutrons in the energy range from 0.4 eV up to 15 MeV. HEND has three ^{3}He neutron proportional counters (Industrial LND 2517 counters.) Each of the three proportional counters is coated by a Cd shield and different thicknesses of a neutron moderator. The counters record thermal neutrons in ^{3}He capture reactions to produce an α particle and a proton. When neutrons enter the detector volume, they lose energy in the polyethylene moderator until they reach the thermal neutron energy range and are registered by the proportional counters. The moderation efficiency of the polyethylene depends on its thickness. The LD detector with the thickest moderator layer (~ 30 mm) is most sensitive to neutrons with energies in the range 10 eV–1 MeV. The MD detector with a 14-mm-thick moderator is sensitive to neutrons in the energy range 10 eV–100 keV. The SD detector with the thinnest (3 mm) moderator is sensitive to neutrons with energies from the cadmium threshold of 0.4 eV to 1 keV. The combined response of the three ^{3}He neutron proportional counters yields data for neutrons in a broad energy range from 0.4 eV to1 MeV.

The scintillator block of the HEND neutron detector is used to detect neutrons with energies greater than 1 MeV. The high energy detector is an inner scintillator of organic stylbene (or stilbene). The inner scintillator detects high-energy neutrons by flashes of light from recoil protons knocked out of the organic crystal lattice by neutrons. In space the organic scintillator may also detect primary protons from cosmic rays. Cosmic-ray electrons and secondary electrons produced by gamma-ray photons are also detected in the stylbene. To separate proton pulses from electron pulses, an electronic separation circuit was specially designed for HEND. The separation is based on the measurable difference between time profiles of scintillation light from protons and electrons. The efficiency of this separation corresponds to one false separation of a proton-based count from 2000 electron-based counts. The stylbene scintillator also contains an external scintillator with a CsI crystal for detection of charged particles and gamma-rays above 30 keV. This detector provides the digital veto signal for anti-coincidence rejection of protons, which could be detected as proton-based counts.

The HEND instrument collects five new neutron spectra from five different energy ranges approximately every 20 seconds, 360 times per orbit, resulting in approximately 4200 neutron spectra per energy range to be collected each day. The ~20 second collection interval,

corresponding to 1-degree on the planet's surface, was chosen due to data transfer rate limitations. Once HEND spectra are collected they are stored on the spacecraft and held for periodic download. The HEND spectra and telemetry data are downloaded periodically from the spacecraft for receipt by the Deep Space Network and insertion into the Jet Propulsion Laboratory's (JPL) Telemetry Data System (TDS). The UA queries the TDS for the most recent telemetry dataset and retrieves the data with a process that translates data packets and examines instrument health via messages. Data are output to a spooler that passes it to both the UA database ingest process and to IKI. The UA ingest process inputs raw HEND data into the UA database. IKI maintains a separate data repository that is used to process the HEND Planetary Data System (PDS) data products.

Timing and spacecraft spatial information are calculated for each HEND collection interval. UTC time is calculated from the spacecraft event time (sc_ev_time, time at the middle of the collection interval in 256th seconds) by a SPICE function. The spatial portion of the collection interval is calculated using other SPICE routines. The returned values are the spatial elements of an observation, including latitude and longitude at the mid-point of the observation.

During each collection interval the HEND instrument collects five neutron signals from four independent detectors, whose response functions are sensitive to different energy regions. Raw neutron counts are reported as a 16-channel spectrum for each of the four detectors. Raw neutron counts are reported as the sums of channels 1-16 in the SD (Small Detector), MD (Medium Detector), and LD (Large Detector). The inner scintillator records two neutron signals, LO and HI. The raw neutron counts for the LO and HI signals are reported as the sum of channels 1-4 and 5-15 respectively, of the HEND neutron spectrum.

A spacecraft background is calculated for each neutron signal in a collection interval. The background term reported for each collection interval is a combination of the galactic cosmic-ray flux induced spacecraft background and a spacecraft orbital geometry term to account for the shadowing by the planet of the galactic cosmic-ray flux. The collection interval's background subtracted counts are simply the raw HEND counts minus the background counts for each signal. Once the background subtracted counts are known for each signal in the collection interval, a determination is made as to the suitability for further processing of the collection interval's data. If the data was collected during a time with high solar activity the collection interval is marked as "bad", and is excluded from further processing.

All "good" background subtracted count values for each of the five neutron signals (SD, MD, LD, LO, HI) are then temporally and spatially binned to compare seasonal changes in the neutron flux. The temporal binning is 15-degrees of solar longitude (L_S) and the spatial binning is a grid of 5-degrees latitude by 5-degrees longitude. The averaged counting rate is then normalized by the average counting rate from the Solis Planum region of Mars defined as 245E to 295E and 15S to 55S. The final normalized average counting rates for each signal are calculated by dividing the average counting rate by the signal specific Solis Planum normalization.

The conversion of normalized counting rates to neutron fluxes requires knowledge of the efficiency of each of the neutron detectors. Efficiency functions, derived from model calculations and direct calibrations, describe the response of each of the four HEND detectors, SD, MD, LD, and the inner scintillator, to bombardment by neutrons. The combined results of the numerical simulations and the experiments yield detector specific efficiency functions. The number of neutrons observed in a given energy interval can be calculated by performing a model depended deconvolution of the HEND counting rate data and an estimate of parameters that describe the shape of the neutron spectra within the energy range. In this study it is assumed that epithermal and fast neutron spectra can be described by a power law function. The observed counting rate data for each HEND detector in each 5x5-degree latitude longitude map cell is fit with the power law function. The power law fit parameters are used to estimate the actual neutron flux [$n/(cm^2 \cdot sec$] on the Odyssey orbit in different energy ranges of epithermal and fast neutron flux for each 5x5 degree map cell.

2. LEVEL 0 PROCESSING- SPACECRAFT DATA RECEIPT AND STORAGE

2.1. GRS_TL

GRS_tl is the process by which telemetry data down-linked from the Odyssey spacecraft is transferred from the JPL TDS to the UA and prepared for ingestion into the UA GRS database. The GRS_tl program is designed to receive input data from any of a number of sources, strip out the GRS specific data, then output that data in the requested format. In the case of telemetry data, a process on the JPL Spacecraft Operations Processing Computer (SOPC) called *stot* retrieves selected Standard Format Data Unit (SFDU) packets from the TDS via a query server, and sends the retrieved SFDU packets to a socket. A connection is made between the socket and GRS_tl, and packet data is passed to GRS_tl.

The stream of SFDU data packets are read in from the socket. The SFDU packet consists of a primary label, an aggregate header (Compressed Header Data Object, CHDO), up to 4 headers (Primary [required], secondary, tertiary, quaternary), and an optional data CHDO. The primary label and headers are stripped from the packet and are written to a file "SFDU.hdr." The remaining information is a Consultative Committee for Spacecraft Data Systems (CCSDS) packet, consisting of header information and data. The CCSDS headers are removed and written to a file "CCSDS.hdr." The remaining data is then in the form of a GRS packet, and includes the data as output by the GRS instrument suite. The GRS data packets consist of a telemetry header structure, a data type specific data structure, and an appended checksum. The last step in the process is to convert the GRS data packets to Bench Checkout Equipment (BCE) type packets. This is done by stripping the telemetry header from the GRS packet and replacing it with a "common header" structure followed by the data type specific data structure. Any needed regrouping or decompression of data occurs in the translation from GRS to BCE data format.

Data with an invalid telemetry header is flagged as "invalid header." If the checksum is not correct, then the packet is flagged as "bad checksum." The BCE formatted data are sent either to a data spooler (similar to a print spooler) to wait for database ingestion or written to files. If BCE

output is written to files, it is placed in a Central Electronics Box (CEB) Telemetry structured directory which can then be used for data validation.

GRS_tl can also be used to translate data from one packet type to another. The input data stream can consist of SFDU packets, CCSDS packets or GRS/CEB data packets. The packets are read, parsed, and translated to an output packet format. Output types can be SFDU, CCSDS, GRS data or BCE formatted packets. The output packets can then be sent to a socket and/or written to a file. The only restrictions on data type transformation are that BCE packets can not be used as GRS_tl input, and the data types can not be "up converted" (e.g. CCSDS packets can not be transformed into SFDU packets.)

2.2. GRS DISPLAYS

The GRS Displays software is a collection of Interactive Data Language (IDL) programs called by a main routine that provides users access to 20 different GRS data display types. IKI uses GRS Displays to retrieve HEND and spacecraft engineering telemetry data via an internet socket from GRS_tl, a UA Solaris server. The GRS Displays program “save telemetry” function is then used to generate BCE formatted files in a CEB telemetry structured data directory on the local file system. The locally stored (at IKI) telemetry data files are used as a repository for further data processing.

3. LEVEL 1-A PROCESSING – TIMING AND SPATIAL INFORMATION

3.1. SPICE PROCESSES

Table 1. SPICE Kernel Definitions

Kernel Name	Description
SPK	Space vehicle ephemeris (trajectory)
PcK	gravitational model of Mars, Mar_IAU_2000
IK	Instrument information, none applicable to GRS
CK	Instrument platform (e.g. spacecraft) attitude
FK	Definitions of and specification of relationships between reference frames (coordinate systems)
LSK	Leapseconds Tabulation, Used for UTC <--> ET time conversions
SCLK	Spacecraft Clock Coefficients, Used for SCLK <--> ET time conversions

The Navigation and Ancillary Information Facility (NAIF) Node of the Planetary Data System (PDS) collects and maintains the SPICE information system. SPICE (Spacecraft, Planet, Instrument, C-matrix, Events) is a means for providing scientists with geometric and event data and related tools, useful in the interpretation of science instrument observations returned from planetary spacecraft. SPICE data files, called kernels, exist for spacecraft trajectory (S); planet ephemeris and associated physical and cartographic constants (P); instrument information,

including mounting alignment and other relevant geometric information (I); orientation of spacecraft structures upon which science instruments are mounted (C); and spacecraft and ground data system events, both planned and unplanned (E) (NAIF, http://pds.jpl.nasa.gov/naif.html). Table 1 is a description of each of the SPICE kernel files.

The SPICE toolkit, provided by NAIF, contains a collection of sub-routines that allow an exchange of information between GRS data and SPICE kernel information. For HEND data processing, the SPICE kernel information is used to convert spacecraft times to UTC times and to calculate the spatial properties of a collection interval. The spatial properties include the latitude, longitude and orbital position at the mid-point of the collection interval.

4. LEVEL 1-B PROCESSING – BACKGROUND SUBTRACTED DATA

During each collection interval the HEND instrument collects five neutron signals from four independent detectors, whose response functions are sensitive to different energy regions. The raw HEND data are reported as 16-channel energy spectra for each of the four detectors. Raw HEND counts for the three ^{3}He proportional counters, SD (Small Detector), MD (Medium Detector), and LD (Large Detector), are simply the sum of counts detected in channels 1-16 of the energy spectra recorded for each detector. The inner scintillator (organic stylbene detector) records two neutron signals, LO and HI. The raw neutron counts for the LO and HI signals are the sum of channels 1-4 and 5-15 respectively, of the HEND inner scintillator energy spectrum.

The total number of neutron counts recorded by each detector contains components from both Mars and the Odyssey spacecraft. In order for the HEND data to be scientifically useful in describing Martian surface characteristics the local spacecraft background must be removed from the HEND neutron signals.

4.1. BACKGROUND SUBTRACTION

The Mars Odyssey spacecraft is a relatively massive body which produces secondary nuclear radiation under bombardment by the galactic cosmic-ray flux. Orbital neutron measurements made by the HEND instrument aboard Odyssey contain a contribution from the spacecraft, called the spacecraft background. The spacecraft background was determined by measuring the number of neutron counts recorded during nominal collection intervals in the HEND detectors during the cruise and aerobraking phases of the mission when the spacecraft was far from both Earth and Mars. The average number of counts per collection interval in each neutron signal is taken as the isotropic galactic cosmic-ray flux induced spacecraft background.

The isotropic galactic cosmic-ray induced background is only an approximation of the spacecraft background. When the spacecraft is in an orbit close to Mars, the planet partially shields the spacecraft from the galactic cosmic-ray flux. The partial shielding decreases the number of galactic cosmic-rays hitting the spacecraft, therefore decreasing the secondary nuclear radiation produced causing a decrease in the spacecraft background counts. This decrease in background counts per measurement interval is taken into account by multiplying the isotropic galactic

cosmic-ray flux induced background by $(1 - \Omega(t)/4\pi)$ where $\Omega(t)$ is the solid angle subtended by Mars from the current point in the spacecraft orbit.

The equation used to estimate the background subtracted signal $\mathbf{S_i}$ for each HEND detector in the *i*-th measurement interval is:

$$S_i = C_i - B_i \cdot \frac{4\pi - 2\pi \cdot \left(1 - \cos\theta^i_{Mars}\right)}{4\pi} \qquad (1)$$

where

$\boldsymbol{C_i}$ – measured counts during *i*-th collection interval in given detector in given set of energy channels,

$\boldsymbol{B_i}$ – counts from isotropic galactic cosmic rays in *i*-th collection interval in given detector in given set of energy channels (measured far away from Mars during cruise and aerobraking mission phases) ,

$\boldsymbol{\theta^i_{Mars}}$ – angular radius of Mars as seen from Odyssey during *i*-th collection interval,

$\boldsymbol{S_i}$ – background subtracted signal in *i*-th collection interval calculated for given detector in given set of energy channels.

The galactic cosmic-ray induced spacecraft background is removed from every measurement interval, resulting in a time-series of background subtracted measurements of each of the five HEND neutron signals; SD, MD, LD, HI and LO.

4.2. EXTRACTION OF SOLAR PARTICLE EVENTS

Once the time-series background subtracted data have been produced for each of the five HEND signals, the data is examined to determine if data collection occurred during a solar particle event. Solar particle events (SPEs) significantly influence the HEND detectors' counting rates, often increasing the counting rates by several orders of magnitude. Any data collected during times of intense solar activity are flagged and excluded from further routine data processing, as the goal of the routine data processing is to create a data set that allows examination of the temporal and spatial changes in Martian neutron albedo over time.

The exclusion of data collected during SPEs is based on visual inspection of the data combined with information from Earth observation of solar activity (i.e. GOES spacecrafts). The visual inspections and comparisons with other data sets do not guarantee that every collection interval that has been influenced by heightened solar activity has been excluded. It is possible that weak traces of SPEs may remain in the data.

5. LEVEL 1-C PROCESSING – SPATIALLY AND TEMPORALLY BINNED DATA

5.1. AVERAGED NORMALIZED RELATIVE COUNTING RATES

Background subtracted, non-SPE influenced time series data are used to create temporally and spatially binned counting rate data for each of the five HEND neutron signals. The time series data are binned temporally by 15-degrees of solar longitude (L_S) and spatially by 5-degrees of latitude and 5-degrees of longitude.

The creation of spatially averaged counting rates requires the time series collection interval data to be distributed between the 5x5 latitude longitude map cells. The time series data distribution is accomplished by registering each collection interval to the projection of the spacecraft orbital trajectory on the surface of Mars (Figure 1). The spacecraft trajectory projection during a single ~ 20 second collection interval is fit with a straight line.

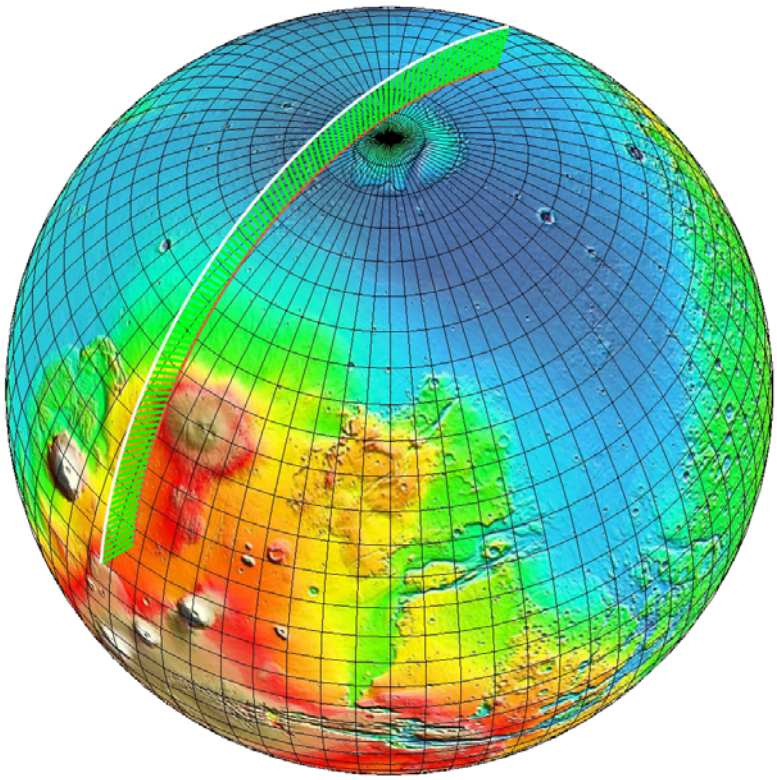

Figure 1. Spacecraft orbital trace.

The projected straight line spacecraft trajectory is used to determine the fraction (***k1, k2, k3***) of the data collection interval that resides inside each 5x5 degree map cell. Equation 2 describes how data collection intervals are split along the length of the trajectory:

$$k_i = \frac{l_i}{L} \tag{2}$$

where

l_i - length of a part of trajectory projection which belongs to i -th map cell,

L – total length of trajectory projection on Martian surface (see fig 2).

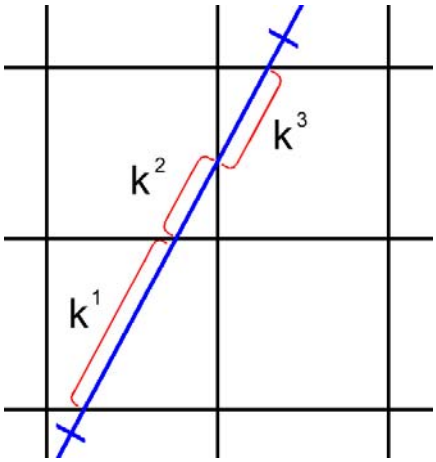

Figure 2. Splitting of the data collection interval between map cells along the projected Odyssey trajectory

The fractions k_i of each collection interval within a given map cell are used to calculate the total number of counts and collection time in each map cell. The following equations describe the process in detail:

$$E_i = \sum_{j=0}^{n} S_j k_{ij} \qquad T_i^{exposure} = \sum_{j=0}^{n} t_j k_{ij} \qquad F_i = \frac{E_i}{T_i^{exposure}} \tag{3}$$

where

S_j – count in j-th collection interval calculated from Equation 1,

t_j – duration of j-th collection interval,

k_{ij} – fraction of j-th collection interval length in i-th map cell,

n – total number of HEND collection intervals within the temporal (15-degrees L_S) interval,

E_i – total counts accumulated in i-th map cell,

$T_i^{exposure}$ – total exposure time for i-th map cell,

F_i – average counting rate in i-th map cell (counts/sec).

5.2. NORMALIZATION TO SOLIS PLANUM

Once average counting rates have been calculated for each 5x5 degree latitude longitude map cell, a normalization to the average counting rate over the Solus Planum region of Mars is applied. The normalization is applied to remove the effects of variations in the Cosmic Gamma-ray (CGR) flux which activates the neutron albedo of Mars and any remaining traces of SPEs not removed by the data reduction algorithms. Variations in the CGR flux and traces of SPEs may cause variations in averaged counting rates of tens of percents. The counting rate variations caused by fluctuations in the CGR flux and SPE remains mask the seasonal changes in neutron counting rates caused by changes in Martian surficial composition.

In order to remove the CGR flux variation and SPE effects on counting rates, a normalization to the average counting rate over Solus Planum is performed. The Solus Planum region [(245E, 295E), (15S, 55S)] was chosen because it is one of the driest regions of Mars, and therefore not affected by seasonal changes in neutron counting rates. Neutron signals observed over this region only vary due to fluctuations in the CGR flux and solar activity. Normalization of the entire map by the counting rate value $F_{Solis\ Planum}$ (counting rate observed above Solis Planum) allows the removal of the CGR flux and SPE components from the averaged counting rates calculated for each map cell. The normalization results in normalized averaged counting rates that are useful for examining the seasonal changes in counting rate due to changes in Martian surficial composition. The normalized averaged counting rate can be calculated as:

$$R_i = \frac{F_i}{F_{Solis\ \ Planum}} \tag{4}$$

Where

R_i – is normalized counting rate in *i*-th map cell for given detector and given set of energy channels

F_i – is counting rate in *i*-th pixel for a given detector and a given set of energy channels calculated by (3).

$F_{Solis\ Planum}$ - is average counting rate in map cells [(245E, 295E), (15S, 55S)].

Statistical errors reported for the normalized averaged counting rates are based on the counting statistics of the raw HEND measurements (**C*i*** in Equation 1, see Appendix 1 for details).

5.3. NORMALIZED MAP VERIFICATION

After the normalized average counting rates for each of the five HEND neutron signals are calculated, they are put through a series of checks to ensure the quality of the data. A first pass test ensures that the mapping algorithm, developed just after the starting of the mapping phase of the mission (February 2002), is generating the expected results. Expected HEND results are maps that show a good correlation with maps produced by the other GRS instruments, the gamma sensor head and the neutron spectrometer. Any unexpected results are closely examined, and the mapping algorithm modified if errors in the code are found. If errors are found in the processing code, all results are re-generated.

Detailed tests are also carried out on each normalized averaged counting rate map. These tests are based on visual analysis, comparison with published maps and analysis of the distribution of the neutron counting rates in neighboring map cells. In the case that the difference between the normalized neutron counting rates of adjacent map cells exceeds 5σ, the counting rates calculated for those map cells will be re-generated and checked at each step in the processing to understand where the processing may have failed.

The final detailed verification of the averaged normalized counting rates is a comparison over time of the normalized averaged counting rates. The counting rates should change in a predictable way due to the seasonal redistribution of atmospheric CO_2 between the Martian poles. Serious errors in the data processing algorithms would show up in these time series analysis as a lack of correspondence between the counting rates over time and the physical laws governing the changing neutron flux from one season to another at a given latitude. Any cases of suspect data will be examined in detail by checking each step in the data processing procedures including background subtraction and extraction of SPEs.

5.4. NEUTRON FLUX MAPS

After the normalized averaged counting rates are calculated, an estimation of the neutron flux at Odyssey orbit can be made. The neutron flux estimation requires an input for the efficiency function of each HEND detector and a model dependent deconvolution of the counts registered in each detector. The results of the model dependent deconvolution are a set of two epithermal and two fast neutron orbital neutron flux seasonal maps. The epithermal maps are divided into two broad energy ranges; 1eV to 100KeV, and 100 KeV to 1 MeV. The fast neutron maps are divided into two energy ranges, 1 MeV to 2.5 MeV and 2.5 MeV to 10Mev.

5.4.1. HEND Detector Efficiency Functions

The first step in estimating the on orbit neutron flux is determining the intrinsic detector efficiency, the ratio of particles detected to the number of particles striking the detector, for each of the neutron detectors. The HEND detector efficiencies were determined by two methods, calculation and direct measurement.

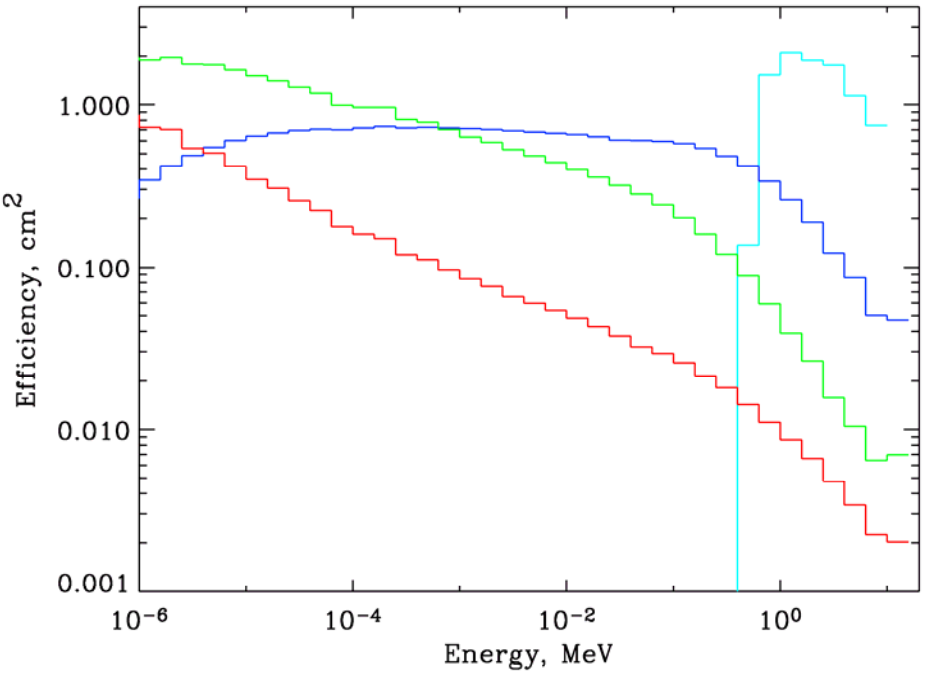

Figure 3. Efficiency functions for the HEND detectors. The cyan line corresponds to the efficiency of inner scintillator stylbene detector. The blue, green and red lines correspond to the LD, MD and SD detectors, respectively.

The detector efficiency functions were calculated using the Monte Carlo N-Particle Extended code (MCNPX). The calculation was performed to yield efficiency functions of each HEND detector that take into account the composition and geometry of the HEND instrument and the surrounding spacecraft mass. In parallel with the MCNPX simulations, a series of experimental

calibration measurements were carried out to understand the quality of the Monte-Carlo simulations. Two types of calibration experiments were performed. In the first experiments calibrated neutron sources with known spectra were measured. The experimental outputs were then compared to the known spectra. In the second set of calibration experiments, neutron measurements were taken while the HEND detectors were exposed to energetic neutron fluxes. The experimental measurements were then compared with the known neutron fluxes. The combined results of both the MCNPX calculations and the calibration experiments were used to yield the efficiency functions presented in Figure 3, which are used in the calculation of on orbit HEND neutron fluxes (see Section 5.4.2)

In the future, additional numerical simulations and calibration experiments will be performed to improve the precision of the HEND efficiency functions. This work will include better simulations of the HEND detectors in the MCNPX calculations and a greater energy range for the experimental measurements. Improvements in the detector efficiency functions will require re-calculation of neutron flux portion of the HEND intermediate data record PDS data product.

5.4.2. Deconvolution of Neutron Spectra

The actual number of neutrons observed in a given energy interval can be calculated by performing a model depended deconvolution of the HEND counting rate data and an estimate of parameters that describe the shape of neutron spectra within the energy range. Neutron spectra covering the broad energy range of 0.4 eV to 10 MeV can be deconvolved using the three ^{3}He proportional counters (SD, MD, LD) and the two signals recorded in the 16-channel stylbene scintillation detector (LO, sums of channels 1-4; HI, sum of channels 5-16).

The observed counting rate in a given HEND detector is:

$$C_i = \sum_j N_j \cdot Eff_j^i \tag{5}$$

where

$\boldsymbol{C_i}$ –counting rate (counts/sec) registered in *i-th* HEND detector (SD, MD, LD, LO sum of low energy channels in stylbene, and HI sum of high energy channels in stylbene),

$\boldsymbol{Eff^i_j}$ – efficiency of *i-th* HEND detector in *j-th* energy interval (cm^2).

$\boldsymbol{N_j}$ – Actual flux of neutrons [n/(cm^2 ·sec)] in *j-th* energy interval.

The neutron flux [n/(cm^2 ·sec)] is calculated as:

$$N_i = \int_{E_j}^{E_{j+1}} \frac{dN}{dE}(E)dE$$

(6)

where

dN/dE – neutron spectra [n/(cm^2 ·sec·MeV)] at the Mars Odyssey orbit.

In this study it is assumed that epithermal and fast neutron spectra can be described by a power law function in the form of:

$$\frac{dN}{dE}(E) = A \cdot E^{-\alpha} \tag{7}$$

with a normalization parameter of ***A*** and a power index of ***α***.

The observed normalized averaged counting rate data for each HEND detector in each 5x5-degree latitude longitude map cell is fit with the power law function. The best fit values of the power law parameters are obtained using a minimization procedure based on Pearson criteria:

$$S(P_j) = \sum_i \left(\frac{\widetilde{C}_i - C_i(P_j)}{\sigma_i} \right)^2 \tag{8}$$

where $S(P_j)$ is the minimizing value and

$\widetilde{C}_i$ –observed counting rate in *i-th* HEND detector (Equation 3),

$C_i(P_j)$ – model predicted counting rate by Equation (5) in *i-th* HEND detector for given set P_j of parameters **A** and **α**,

σ_i – measurement error including static error of counts and accuracy of approximation of efficiency function.

***i* =1, 2..5** correspond to SD, MD, LD, LO and HI.

The final products of the minimization procedure are the best fit values of parameters $\mathbf{A_k}$ and $\boldsymbol{\alpha_k}$ for each 5x5 degree map cell. These parameters are used to estimate the actual neutron flux N_k [n/(cm^2 ·sec] at the Odyssey orbit in different energy ranges of epithermal (1eV-100 KeV, 100 KeV-1 MeV) and fast neutrons (1 MeV-2.5 MeV, 2.5 MeV-10Mev):

$$N_k = \int_{E_{bottom}}^{E_{upper}} \frac{dN}{dE}(E, A_k, \alpha_k)dE \tag{9}$$

where E_{upper} and E_{bottom} the borders of given energy range.

5.4.3. Verification of Neutron Fluxes

The Pearson minimization procedure best fit parameters $\mathbf{A_k}$ and $\boldsymbol{\alpha_k}$ that describe the shape of the neutron spectra in a given *k*-th map cell are compared with the results of an MCNPX simulation of neutron leakage fluxes in order to verify that the best fit parameters adequately describe the neutron spectra and are useful for calculation of neutron fluxes. The MCNPX simulations provide an energy spectrum of neutrons above a model area that contains a model composition of the regolith, the thickness of atmosphere and the average elevation of this area.

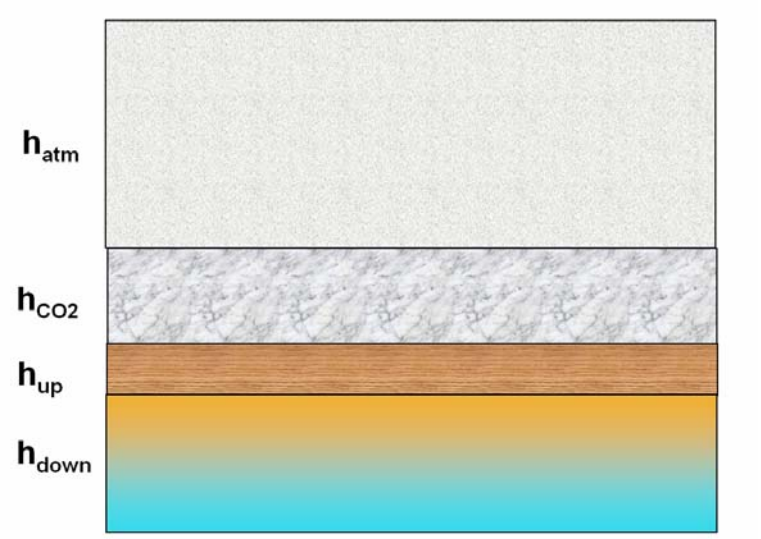

Figure 4. The schema of the model with double-layered subsurface for numerical calculations for leaking neutron flux.

A two-layer model of the subsurface is used to calculate the neutron leakage flux from the layer of neutron production, which is based on 4 sub-layers with different compositions (Figure 4). The top model layer (bright gray) is the Martian atmosphere with the thickness $\mathbf{h_{atm}}$, which varies according to the NASA Ames Mars General Circulation Model (GCM). The second layer, with the gray structure, is the winter surface deposition of CO_2. The thickness of this layer is variable. The third layer (brown layer) is the upper most layer of dry ground soil with $\boldsymbol{\zeta_{up}}$ mass % of water and (100 - $\boldsymbol{\zeta_{up}}$) mass % of soil with Pathfinder composition. The third layer has a

variable thickness, $\mathbf{h_{up}}$. The bottom layer (brown to blue layer) has a soil with $\zeta_{\mathbf{down}}$ mass % of water and (100 - $\zeta_{\mathbf{down}}$) mass % of soil with Pathfinder composition. The bottom layer thickness is $\mathbf{h_{down}}$ >> 2 m. The regolith model parameters were estimated for a frost-free surface with no CO_2 frost on the Martian surface. Once the regolith parameters are set to simulate a given map cell, the MCNPX simulations are run to produce the orbital neutron spectra above the selected map cell. Comparison between the MCNPX model produced spectra and the power law described spectra are used as a validation of the orbital neutron fluxes obtained by deconvolution of the observed normalized averaged neutron counting rates.

The results of Monte-Carlo simulations for 74 northern regions (Latitude > 60N), 15 equatorial regions (20S > Latitude <2 0N) and 98 southern regions (Latitude > 50S) have been compiled for comparison with the power law produced neutron spectra. The results of these comparisons show good agreement and are presented in Figure 5.

In general, the Monte-Carlo simulations, with variation in the atmosphere and regolith parameters, are the best way to estimate the surficial and orbital neutron flux of Mars. However, running the MCNPX models is time intensive. The significantly shorter computation time and the general agreement between the MCNPX generated results and the results of the power law described neutron spectra is a strong argument for using the power law approximation to calculate the actual neutron flux at Mars Odyssey orbit.

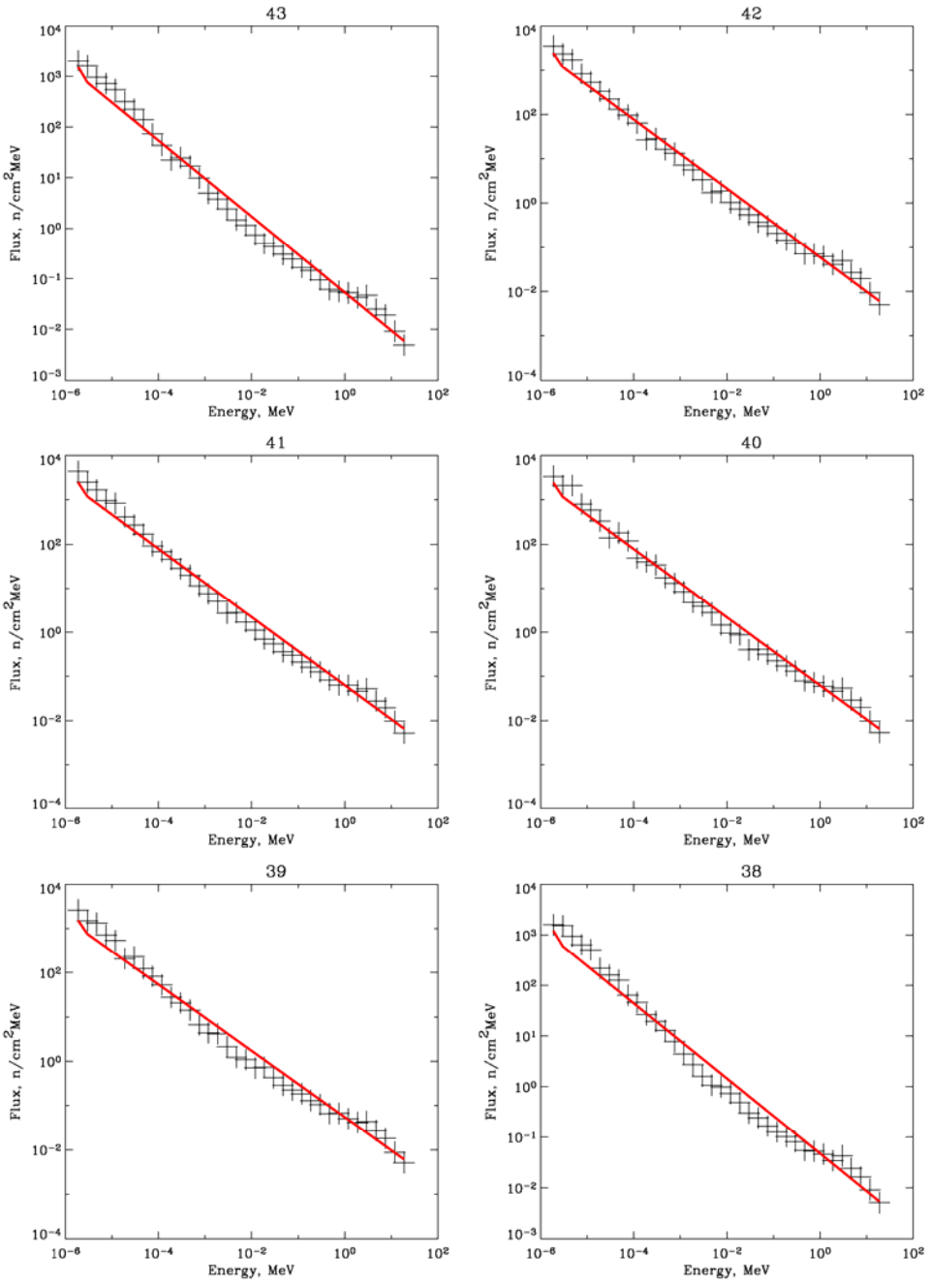

Figure 5. Example of comparison between Monte-Carlo simulations of orbital spectra by MCNPX code (shown as black crosses) and power law approximation (red line).

6. APPENDIX 1 - CALCULATION OF NORMALIZED COUNTING RATE UNCERTAINTIES

The uncertainty in the normalized AHD counting rates are calculated as given below:

Step 1:

For given pixel of map *i* (5x5 degree) the total accumulated signal E_i (counts), total accumulated exposure time T_i (seconds) and flux F_i (counts/sec) are calculated according following formulas:

$$E_i = \sum_{j=0}^{n} S_j k_{ij} = \sum_{j=0}^{n} C_j k_{ij} - \sum_{j=0}^{n} B_j k_{ij} \qquad T_i^{exposure} = \sum_{j=0}^{n} t_j k_{ij} \qquad F_i = \frac{E_i}{T_i^{exposure}}$$

Where $\{C_j\}$, $\{B_j\}$ are sets of counts and background estimations observed in individual data accumulation intervals (~20 sec) above a given map's pixel; n – number of individual accumulation intervals which crossed the given map pixel *i* . The set $\{k_{ij}\}$ contains coefficients which take into account a part of an individual data accumulation interval lying within a given pixel. The set $\{t_j\}$ contains durations of individual data accumulation intervals.

Assuming that the counting statistic in a given pixel of the map follows Poisson statistics, the uncertainty of F_i may be defined by the following equations:

$$\delta E_i = \sqrt{\sum_j C_j k_{ij}}$$

$$\delta F_i = \frac{\delta E_i}{T_i^{\exp osure}}$$

Step 2:

The normalization value $F_{Solis\ Planum}$, the average counting rate observed above equatorial regions, [(245E, 295E), (15S, 55S)], is calculated. The estimation of the normalization value $F_{Solis\ Planum}$ and its uncertainty $\delta F_{Solis\ Planum}$ is based on the algorithm presented at step 1.

Step 3:

The normalized counting rates R_i and its uncertainties are estimated with the following equations:

$$R_i = \frac{F_i}{F_{SolisPlanum}}$$

$$\delta R_i = \sqrt{\left(\frac{\delta F_i}{F_{SolisPlanum}}\right)^2 + \left(\frac{F_i}{F_{SolisPlanum}^2}\delta F_{SolisPlanum}\right)^2}$$

Verification:

There is another way to estimate the normalizing value and its uncertainty in a given pixel of the map. The second method substitutes the following equations into step 1:

$$F_i = \frac{\sum_{j=0}^{n} f_{ij}}{n} = \frac{\sum_{j=0}^{n} \frac{S_j k_{ij}}{t_j k_{ij}}}{n}$$

$$\sigma_i = \sqrt{\frac{1}{n-1}\sum_{j=0}^{n}\left(f_{ij} - F_i\right)^2}$$

$$\delta F_i = \frac{\sigma_i}{\sqrt{n}}$$

The final value R_i and δR_i in this approach may be estimated using step 2 and step 3.

Testing

DHD and AHD data products are created independently by different programs. It gives us possibility to perform rough test of AHD data using DHD data. To do this, a time interval February 21, 2002 – March 21, 2002 and a map pixel having coordinates: Lon=[0^o,5^o]; Lat=[0^o,5^o] are selected for comparison. Such selection is based on the following reasons:

DHD data does not contain the $\{k_{ij}\}$ coefficients which are an internal product of AHD software. As mentioned in step 1 these coefficients take into account a part of an individual data accumulation interval (~20 sec) which belongs to the given pixel of the map. This coefficient starts to play an important role for polar and near polar pixels because of their small sizes. The correction caused by $\{k_{ij}\}$ is not so significant for equatorial pixels. Thus, this pixel and timer period are appropriate choices for comparing AHD data and DHD dataset.

Table 2 contains estimations of normalized counting rates (Lon=[0^o,5^o]; Lat=[0^o,5^o].) for SD_RATE, MD_RATE, LD_RATE, IN_SC_LOW_RATE and IN_SC_HIGH_RATE fields in the February 21, 2002 - March 21, 2002 AHD dataset. The values marked as (AHD) are simply taken from the AHD dataset. The values marked as (DHD) are estimated using a DHD dataset and algorithms in step1-step3. The values marked as (SA_DHD) are estimated using DHD

dataset and algorithm described in second approach. The correspondence between these approaches looks quite good including mean values and its uncertainties.

Table 2

Field in AHD dataset	$F_{SolisPlanum}$(AHD)	R (AHD)	$F_{SolisPlanum}$(DHD)	R (DHD)	$F_{SolisPlanum}$(SA_DHD)	R (SA_DHD)
SD_RATE	0.049	0.51±0.18	0.049	0.47±0.17	0.049	0.47±0.14
MD_RATE	0.216	0.59±0.08	0.217	0.60±0.07	0.217	0.60±0.07
LD_RATE	0.243	0.53±0.08	0.244	0.58±0.08	0.244	0.58±0.08
IN_SC_LOW_RATE	0.290	0.87±0.09	0.291	0.88±0.08	0.291	0.88±0.09
IN_SC_HIGH_RATE	0.182	0.94±0.13	0.188	1.01±0.12	0.188	1.01±0.11

7. APPENDIX 2 - CORRECTIONS TO HEND AHD & DHD DATA PRODUCTS

The HEND data products have been reprocessed to make corrections of background influenced with changes of Cosmic Gamma Ray flux as a function of solar cycle. It is known that flux of CGR is not constant and varies with time during solar cycle (see for example Masarik & Reedy, JGR, 101, 18891-18912, 1996.) To consider this phenomena we have selected HEND data above Solis Planum and tried to fit it with numerical modeling of Martian soil with homogeneous distribution of water content equal to 2% by mass fraction for different season interval starting from February, 2002 (beginning of mapping) until end of 2005. The free parameter of the model was flux of CGR which we input in our numerical model to simulate neutron production in the Martian soil. The results of modeling are shown on Figure 7.1 where we have presented relative changes of CGR flux in comparison with beginning of mission.

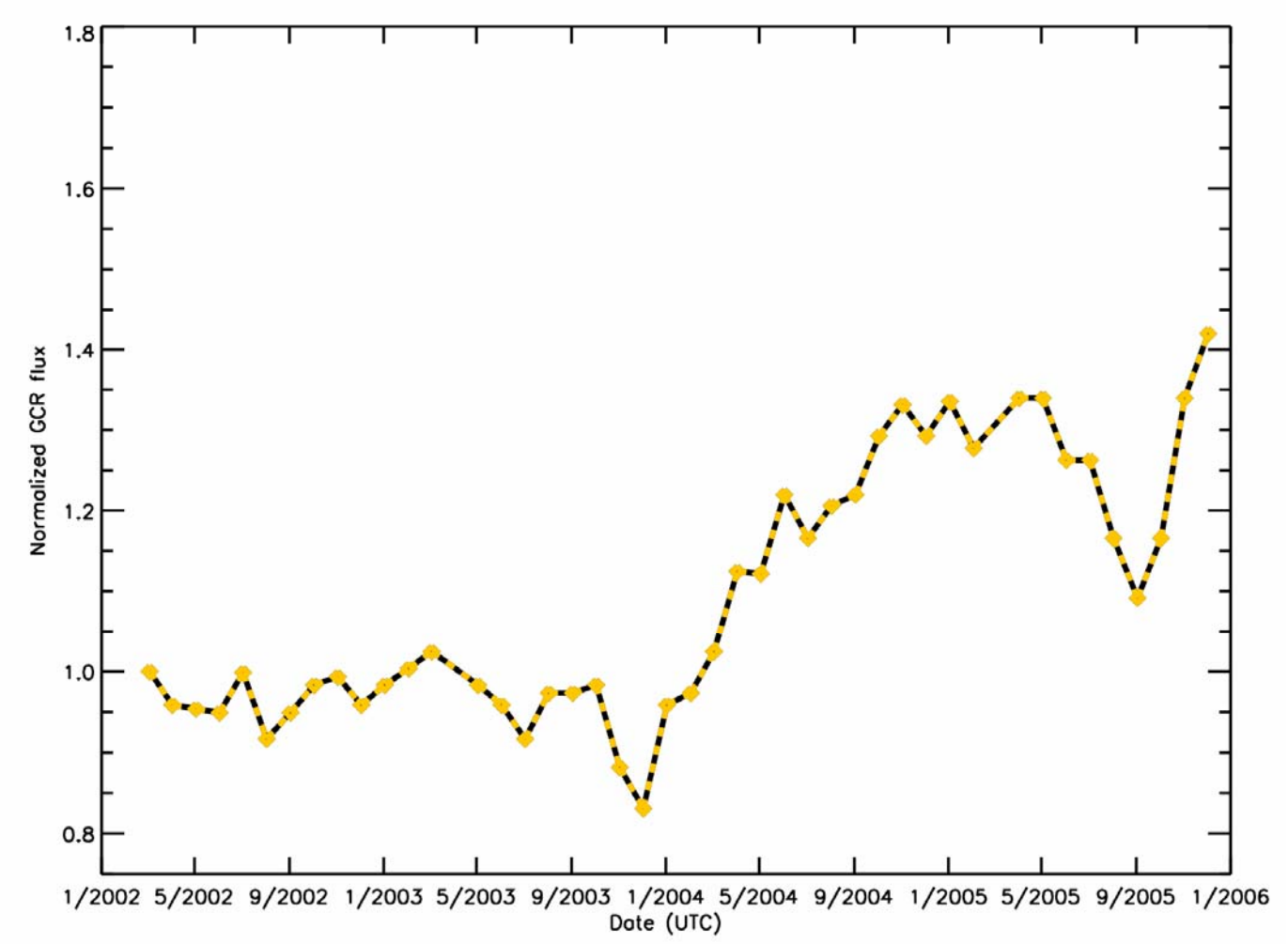

Figure. 7.1 Relative changes of CGR flux during the Odyssey mission as revealed by HEND data analysis.

The CGR value presented on the Figure 7.1 is used in equation 7.1 (similar to equation 1 presented earlier in this document) which is used to determine the background subtracted signal S_i for each HEND detector in given *i*-th measurement interval (frame):

$$S_i = C_i - \widetilde{B}_i \cdot \frac{4\pi - 2\pi \cdot \left(1 - \cos\theta^i_{Mars}\right)}{4\pi} \qquad (7.1)$$

where

$\boldsymbol{C_i}$ – measured counts during *i*-th frame in given detector in given set of energy channels,

$\boldsymbol{B_i}$ – counts from isotropic galactic cosmic rays in *i*-th frame in given detector in given set of energy channels (measured far away from the planet during aerobraking stage and cruise stage) ,

$\boldsymbol{\theta^i_{Mars}}$ – angular radius of Mars as seen from Odyssey during *i*-th frame,

$\boldsymbol{S_i}$ – background subtracted signal in *i*-th frame defined for given detector in given set of energy channels.

In this formula all CGR flux corrections taken from Figure 7.1 are included inside of coefficient $\widetilde{B}_i = B_i \times K(t)$ where B_i is the old coefficient (Equation 1) and K(t) coefficient taken from Figure 7.1 as a function of time.

From the Figure 7.1 it can be seen that major corrections to the HEND PDS data products begin at about September, 2003 when CGR flux begins to deviate from the value observed at the beginning of the mission.